Pollutant transport processes in the Odiel River (SW Spain) during rain events.

Carlos Ruiz Cánovas [a b], Manuel Olías [b], Aguasanta Miguel Sarmiento [c d], Jose Miguel Nieto[d], Laura Galván [b]

a) Department of Geosciences. Institute of Environmental Assessment and Water Research (IDÆA-CSIC). c/ Jordi Girona, 18-26, 08034 Barcelona, Spain.

b) Department of Geodynamics and Palaeontology, University of Huelva (UHU). Facultad de Ciencias Experimentales, Avenida 3 de Marzo s/n, 21071 Huelva, Spain.

c) Department of Analytical Chemistry, University of Cádiz, (UCA). 11510, Puerto Real, Cádiz, Spain

d)) Department of Geology, University of Huelva (UHU). Facultad de Ciencias Experimentales, Avenida 3 de Marzo s/n, 21071 Huelva, Spain.

ABSTRACT

An understanding of pollutant processes in rivers under different hydrological conditions is essential to assess its long-term evolution. This is especially relevant in Mediterranean rivers during rain events, when most of the water, suspended particulate matter (SPM) and pollutants are delivered. This study investigates the hydrochemical changes and pollutant fluxes in the Odiel River (SW Spain) during rainy conditions. For this purpose, high-resolution sampling (6 h) was performed to monitor dissolved and total concentrations of pollutants. During the rises in discharge, most dissolved elements had decreased concentrations due to the dilution effect of runoff waters and Fe precipitation

processes. However, the particulate concentrations of some elements (As, Fe, Pb, Cr, Ti, V and Ba) increased due to Fe-rich sediment remobilization, and to a lesser extent, direct precipitation. A two end-member mixing model applied to the collected data showed that the contribution of freshwaters was around 85-98% of the total discharge, highlighting the importance of mining lixiviates in the deterioration of Odiel water quality. An innovative methodology was applied to estimate dissolved and total pollutant loads, based on the relationships between a) dissolved concentrations and electrical conductivity (EC) and; b) total concentrations and river flow. The importance of particulate metal transport during rain events in the Odiel River was significant. The total transport of Fe was 37 times higher than dissolved Fe, was almost 7 times higher for Pb and 5 times higher for Cr, while As (1.1 t) was totally transported by particulate matter.

1. INTRODUCTION

The Odiel River (SW Spain) drains one of the most famous sulfide-mining regions in the world: the Iberian Pyrite Belt (IPB), and contains original reserves in the order of 1700 Mt divided into more than 80 massive sulfide deposits. Sulfides are stable under reducing conditions, however, when they are exposed to atmospheric conditions they undergo oxidation, releasing acidity, sulfates, Fe and accessory metals into the environment. This process, known as acid mine drainage (AMD), is a major worldwide environmental problem associated with the mining of sulfide and coal deposits. Owing to its mineral richness, the IPB has been extensively exploited since 3000 B.C. for the extraction of gold, silver and copper (Nocete et al., 2005), and as a result enormous amounts of mining wastes have been deposited within the Odiel watershed. The long-lasting effects of mining pollution in the IPB have given rise to deteriorating water quality in the Odiel River (Sainz et al., 2004; Cánovas et al., 2007; Nieto et al., 2007; etc.). According to

48 Sarmiento et al. (2009), 37% of the total length of the Odiel watershed is affected by
49 AMD, which results in huge pollutant transport into the Odiel Marshlands (i.e. 2847 t/a
50 of Fe, 2612 t/a of Zn, 23 t/a of As; Olías et al., 2006).
51
52 Most published works on pollutant transport deal with annual budgets without
53 considering the study of rain events. These type of events need to be studied with a high
54 temporal sampling resolution as geochemical and hydrological factors have a great
55 variability during storms. Detailed studies on the transport of contaminants by the Odiel
56 River during rain events have not previously been reported. Some studies have been
57 performed on the adjacent Tinto River which have highlighted the importance of these
58 events in metal transference from rivers to oceans (Cánovas et al., 2008, 2010), although
59 they only deal with dissolved metal transport
60
61 In this sense, most studies on AMD river systems focus on dissolved pollutants, and not
62 on frequent particulate metal fluxes. Metal and metalloid transport in contaminated river
63 systems requires understanding and the quantification of particulate transport during
64 floods (Coynel et al. 2007). This is particularly relevant in Mediterranean rivers, where a
65 great part of the annual suspended particulate matter (SPM) load is delivered during rain
66 events. On the other hand, the boundary of metal partitioning between the dissolved and
67 particulate phases has been traditionally unclear. Most studies have relied on filtration
68 through 0.45 μm membranes to determine the true dissolved phase, despite including
69 clusters or aggregates, the precursors of colloids. In the last few years, smaller sizes have
70 been used to discriminate the truly dissolved phase, and many works have reported
71 dissolved concentrations after filtering through 0.20 or 0.10 μm membranes The present
72 paper provides high-frequency data on discharge and both dissolved (through 0.10 and

0.45µm filters) and total concentrations in the Odiel River during a rain event occurred in an especially dry period. Therefore, the aims of this work were to study in detail the pollutant processes during rain events in the Odiel River, the influence of the filter size on the metal estimates and the fate of metals between the dissolved and particulate fractions.

2. STUDY AREA

The Odiel basin is located in the southwest of the Iberian Peninsula (Fig. 1) and is the largest drainage basin in Huelva Province, with an area of about 2300 km^2. The Odiel River starts in the Sierra de Aracena and, together with the Tinto River, flows into a coastal wetland known as the Ría of Huelva estuary. Its annual flow has been estimated to be about 500 hm^3/yr; however, marked variations are frequent due to the Mediterranean climate, which includes long periods of drought and intense rain events. As a consequence of the intense pollution by AMD, this river has been the subject of much research. A review of main hydrological, meteorological and geological characteristics of the Odiel river basin can be seen in Olias et al. (2004), Sainz et al. (2004), Sánchez-España et al. (2005) and Sarmiento (2009).

Figure 1 shows the main mines spoiling into the Odiel River basin. The lixiviates of Cueva de la Mora and Aguas Teñidas old mines flow into the Olivargas reservoir (Fig. 1), where the concentration of the polluted elements strongly decreases due to dilution processes. The reservoir water shows a chemical composition typical of uncontaminated freshwaters (Sarmiento et al., 2008); therefore, these mines were not considered in this study.

98 Table 1 describes the main mines of interest in this work. The contaminant load
99 discharged by the mines was estimated by Sarmiento et al. (2008). Concepción is the first
100 mine to affect the Odiel River (Fig. 1), followed by San Platón, Esperanza, La Poderosa
101 and Riotinto Mines. Of these lixiviates from the Riotinto mine cause most pollution due
102 to a higher discharge and elevated concentrations of toxic elements. These lixiviates flow
103 directly into the Odiel River releasing around 1200 t/y of Zn, 800 t/y of Cu and minor,
104 but important quantities of As, Cd and Pb, annually (Table 1).
105
106 Downstream, other mines which release lixiviates into the river are San Miguel,
107 Angostura, La Zarza, Tinto Sta. Rosa and Sotiel. However, in this zone, the principal
108 contaminant source emanates from the Almagrera dams (Fig. 1). In the Almagrera
109 Industrial Complex, polymetallic sulfide ores are processed by flotation for the
110 production of base metal concentrates (Cu, Pb and Zn). A part of the crude pyrite refuse
111 is processed for the production of sulfuric acid, oleum and Cu sulfate, by roasting and
112 SO_2 recovery. Two tailing ponds were built, one for pyrite cinders and the other for the
113 flotation plant refuse. Pyrite, sphalerite and galena are the main ore components.
114 Chalcopyrite, arsenopyrite, pyrrhotite, stannite, cassiterite, magnetite and gold have also
115 been identified as accessory minerals (García De Miguel, 1990). The lixiviates which
116 emanates from these deposits produce a contamination load into the Odiel river of about
117 4.9 t/y of As, 8.2 t/y of Pb, 400 t/y of Zn and larger quantities of other toxic elements
118 (Table 1). In recent years, a remediation program has been initiated in Almagrera, based
119 on the neutralization of effluents using $CaCO_3$.
120

121 ## 3. METHODOLOGY

122

123 **3.1.Sampling**

124 The sampling site was situated at the stream-gauge station of Sotiel (Fig. 1), belonging to
125 the Andalusian Water Agency. At this point, the river drains an area of around 878 km^2
126 and receives discharges from some of the most important mining complexes within the
127 Odiel catchment (Table 1). Sampling was carried out using a Teledyne ISCO®
128 autosampler, with a sample container holding up to 24 bottles and an outlet pipe made of
129 polyethylene. Samples were pumped by a peristaltic pump, with a scheduled purge stage
130 between samples to avoid cross-contamination. Sample-containing bottles were washed
131 in 10% (v/v) nitric acid and then with milli-Q water (18.2 MΩ) prior to sampling. The
132 sampling period was from 26th January to 2nd February 2006, with a frequency of 6 h
133 between sampling events. Aliquots of each sample were filtered through 0.10 and 0.45
134 μm Millipore® Teflon filters in order to compare the element distribution between the
135 two pore sizes. Colloids are defined as particles from 1 nm to 1 μm in diameter, and as
136 both filters used in this study only covered a limited portion of this size range, this implies
137 that some colloidal particles of smaller diameter were considered dissolved (Langmuir,
138 1997). Samples filtered through both filters were subsequently acidified with suprapure
139 nitric acid Merck® to pH<2 and stored in a refrigerator until analysis. Filters were stored
140 in order to characterize the composition of the solid phases carried by the river over the
141 sampling period.
142
143 In addition, raw samples were collected to determine the total element concentration
144 (dissolved + particulate) using the nitric acid in-bottle digestion procedure proposed by
145 Garbarino and Hoffman (1999). This procedure is a modification of hydrochloric acid in-
146 bottle digestion (Hoffman et al., 1996) used since 1992 by the National Water Quality
147 Laboratory (NWQL) of the U.S Geological Survey (USGS) to determine element

concentrations in raw water samples. An adequate volume of raw water was taken and placed in polyethylene bottles. After adding 1.6 mL of nitric acid for every 50 mL of raw water, each bottle was capped and shaken vigorously, and subsequently heated in an oven for 8 h at 65ºC. After removing from the oven, the samples were shaken vigorously again and an adequate volume of the digestate was filtered through 0.45 μm Millipore® Teflon filters. Finally, the filtered aliquots were stored in a refrigerator until analysis. A reagent blank was prepared with each set of the digested samples.

Temperature, pH, redox potential (Eh) and electrical conductivity (EC) of the samples were measured in the field with portable meters (Hanna Instruments HI 9025 and HI 9033). The instruments were calibrated before carrying out the readings. Redox potential values were corrected to obtain the potential referred to the hydrogen electrode (Nordstrom and Wilde, 1998).

In order to record the hydrochemical changes related to water level variation during the sampling period, EC, temperature and water level were monitored every ten minutes using a Van Essen® Diver datalogger set up at the sampling point. The CTD Diver Datalogger (DI 261) was equipped with pressure and temperature sensors and a four-electrode sensor to measure EC. The air pressure was compensated by means of a Barodiver Datalogger (DI 250). Corrected values for specific EC and water levels were obtained. Rainfall data were obtained from ten different gauges distributed within the Odiel catchment and water discharge was calculated from the water level and the rating curve of the stream gauge station.

3.2. Analysis of dissolved and total concentrations

From all samples taken during the monitoring period, 18 were selected for analysis (Fig. 2A), according to changes observed in EC. The chemical analysis was undertaken at the Central Research Services of Huelva University following a custom-designed protocol specific to waters affected by AMD (Ruiz et al., 2003). Cations were analyzed using Inductively Coupled Plasma Optical Emission Spectroscopy (ICP-AES) on a Jobin Yvon (JY ULTIMA 2) spectrometer. Aluminum, As, Ba, Be, Ca, Cd, Co, Cr, Cu, Fe, K, Li, Mg, Mn, Na, Ni, P, Pb, S, Si, Sr, Ti, V and Zn were determined, although in this work only the most significant cations are presented. A triplicate analysis was performed in order to evaluate the analytical precision, which was below 5% in all cases. In each analysis sequence, blanks were analyzed, and all elements were below the detection limit of the technique (Table 2). The analytical accuracy was confirmed by the analysis of reference materials (NIST-1640).

3.3.Solid phase characterization

In order to study the particulate matter transported by the river over the survey, samples were filtered through 0.45 μm filters which were preserved for the mineralogical analysis of particulate matter. All analyses were performed at the Central Research Services of Huelva University. Particulate matter was characterized by X-ray diffraction (XRD, power method) using a Bruker diffractometer (model S8 Advance). Working conditions were fixed at 12 mm, CuKα monochromatic radiation, 20 mA and 40 kV. Samples were run at 0.125 2Θ/min (3-65º) due to the low crystallinity of Fe colloidal precipitates. Semi-quantitative mineralogical determination was performed with Powder-X version 2004.04 for Windows. Selected solid samples were also observed under field-emission scanning electron microscopy (SEM) using a JEOL JSM-5410 equipped with an energy dispersive system for microanalysis (EDS).

198

199 ### 3.4.Data Treatment

200 With the aim of studying the metal partitioning between aqueous and solid phases, the
201 saturation indices of water samples and the speciation of main elements have been
202 calculated using the geochemical code PHREEQC (Parkhurst and Appelo, 1999). The
203 thermodynamic database of PHREEQC was enlarged with data for the solubility of
204 schwertmannite (Bigham et al., 1996; Yu et al., 1999) and ferrihydrite (MINTEQA2;
205 Allison et al., 1990).

206

207 In order to study mixing processes in the Odiel River during the survey, the code MIX
208 (Carrera et al., 2004) has been used. This software can be freely downloaded from
209 http://www.h2ogeo.upc.es/software/MIX_PROGRAM/index.htm. MIX is a maximum
210 likelihood method to estimate mixing ratios, while acknowledging uncertainty in end-
211 member concentrations. The variables need satisfying some conditions to be suitable in
212 mixing models: exhibit a conservative behaviour and their values must be significantly
213 different in the extreme components. Only elements with a conservative behavior (Al,
214 Ca, Cd, Co, Cu, Mg, Mn, Ni, sulfate and Zn) were used to calculate mixing ratios.
215 Estimations were performed considering fixed end-member concentrations on the basis
216 of the scarce hydrochemical variations in sources observed by Sarmiento et al. (2009)
217 within the humid period.

218

219 ## 4. RESULTS AND DISCUSSION

220 ### 4.1.Results

221 #### 4.1.1. Hydrological context and discharge variations

The rain event studied took place after a very dry period; the Odiel basin averaged less than 200 mm of rainfall during the hydrological year 2004/05. Although near 230 mm were recorded after summer (from October to January) they did not generate high discharges, as a consequence of the low moisture content in the basin soils (Fig. 2A). However, these rainfalls caused the progressive dissolution of salt minerals and the leaching of concentrated pore fluids from spoil heaps in mine sites, resulting in an increase in water mineralization (Fig. 2B). Once these salts and leaching products were fully washed by new rainfalls, higher discharges were recorded and dilution by run-off originated a decrease in water mineralization before the rain event studied (2B).

During the survey, two different rises in discharge were observed (Fig. 2C). Rainfall started on 26th January, although due to its low intensity (4 mm) it had little impact on the river. More intense rainfalls (19 mm) were recorded on 27th January, giving rise to the first increase in river flow. The flow then decreased progressively until the arrival of waters generated by new rainfalls on 28th and 29th January (around 20 mm). This runoff provoked a second rise in flow which peaked on 30th January. Finally, rainfall ceased and the flow decreased progressively up to the end of the survey. The maximum river flow recorded during the study period was 2.3 m^3/s. This value seems to be rather low if compared with the storm events monitored in October 2004 (127 m^3/s) and 2005 (8 m^3/s) by Cánovas et al. 2008 and 2010, respectively, in the adjacent Tinto River. This can be explained by lithological differences between both drainage areas and the intensity of rain events. Although rain events studied in both rivers are performed in similar drainage areas (756 and 878 km^2 for the Tinto and Odiel rivers, respectively) , the Tinto river basin underlain materials mainly composed by volcano-sedimentary rocks with low permeability while in the northern part of the Odiel basin outcrops carbonate rocks with

247 higher permeability, which may reduce the run-off generation in this river reach. On the
248 other hand, the intensity of rainfalls recorded during this study (45 mm) is lower than that
249 recorded in the Tinto River in October 2005 (55 mm) and especially in October 2004
250 (near 150 mm).
251
252 **4.1.2. Hydrochemical variations**
253 Basic statistics of the parameters and analytical results is shown in Table 2. Electrical
254 conductivity (EC) values recorded by the datalogger showed a high correlation (R^2 =
255 0.96) with those taken manually. An increase in pH values was observed during the first
256 discharge rise (from 2.87 to 3.74; Fig. 2D), while EC values decreased from 1600 to 894
257 µS/cm (Fig. 2E). However, EC values recovered slightly over the rising limb as evidenced
258 by the data recorded by the datalogger, which was immediately followed by a new
259 decrease (Fig. 2E). During the falling limb, a progressive increase in EC took place,
260 reaching values even higher than those recorded at the beginning of the survey, while pH
261 decreased (Fig. 2D). During the course of the second discharge rise, a new decrease in
262 EC values and an increase in pH values were observed, reaching the lowest and highest
263 value of both parameters during the survey, respectively (454 µS/cm and 4.11). As in the
264 first discharge rise, the decrease in EC values was also interrupted by a new recovery
265 which would not have been appreciated without installation of the sensor (Fig. 2E).
266 Finally, EC values increased progressively through the falling limb coinciding with a
267 decrease in pH values. The EC recovery observed by the sensor during the falling limb
268 of both discharge rises indicated the arrival of more mineralized waters from an area close
269 to the sampling point, probably from the Almagrera Mine (Fig. 1). Redox potential (Eh)
270 values decreased with the first discharge rise, and fluctuated thereafter (Fig. 2F).
271

If dissolved concentration values obtained after using 0.10 and 0.45 μm filters are compared, no significant differences were found for most of the elements, with an R^2 value close to 1 for Al, Ca, Cd, Co, Cu, Li, Mg, sulfate, Si, Sr and Zn. However, a group of elements showed lower values, such as Fe (0.87), Pb (0.78) and Cr (0.77) due to higher values recorded in the 0.45 μm phase. Figure 3 shows the evolution of the dissolved and total (dissolved + particulate) concentration of some elements during the survey. Regarding dissolved concentrations, a group of elements formed by Al, Cd, Co, Cu, Mn, Si, sulfate (Fig. 3), Mg, and Ni decreased during the discharge peak, and in turn, increased over the falling limb, reaching values even higher than those recorded before the event. Other elements such as Ca, Cr, Fe, Sr, Zn (Fig. 3) and Li also showed this tendency, although their highest values were obtained before the rains. However, there were elements with different behaviors. During the first rain event, Na concentration decreased progressively remaining almost constant thereafter (Fig. 3). On the other hand, Pb concentration increased which coincided with the discharge rises. The same evolution was observed for Ba, although not as evident as that for Pb (Fig. 3). In addition, dissolved concentrations of As were below the detection limit in most samples.

Regarding total (dissolved + particulate) concentrations, some differences among elements were found. On the one hand, As, Fe, Pb, Cr, Ba, Si (Fig. 3), Ti and V had high total concentrations during the survey, peaking during the discharge rises. Among these elements, the most striking was As, with dissolved concentrations below the detection limit in most samples but elevated total concentrations. On the other hand, the majority of elements studied showed little differences between dissolved and total concentrations. Among them, two different groups of elements were identified; i) the first, formed by Cd, Co, Zn, Ca, Mn, Na (Fig. 3) and Mg, which did not exhibit any differences between

297 dissolved and total concentrations, and ii) the second, formed by Al, Cu, Sr, sulfate (Fig.
298 3) and to a lesser extent, Li and Ni, with little presence in the particulate phase, except
299 during the discharge peaks when the total concentration exceeded the dissolved
300 concentration.
301
302 **4.2.Discussion**
303 **4.2.1. Dissolved concentrations**
304 The hydrochemistry of the Odiel River during the survey seemed to be strongly linked to
305 the intense water-rock interactions that take place in its catchment. The similarity in
306 trends observed between elements commonly contained in sulfides and others not present
307 in these sulfides (Fig. 3), indicates a variety of geochemical reactions. On the one hand,
308 intense sulfide oxidation processes release Fe, sulfate and accessory metals (Cu, Cd, Co,
309 Zn, etc.) into the Odiel fluvial network. On the other hand, the dissolution of gangue
310 minerals and hydrolysis reactions of aluminosilicates on the riverbed provoke the
311 mobilization of Al, Mg, Ca, Sr, Si, Li, etc. Both groups of elements are put into dissolution
312 due to strong water-rock interactions (i.e. sulfide oxidation, host rock dissolution);
313 however they may follow different trends due probably to geochemical controls. Calcium
314 and Sr have a similar behavior which seems to be linked to lithological factors; Sr can
315 replace Ca in a wide range of minerals due to their similar ionic radii (Dill, 2010). In turn,
316 Ba which also has a similar ionic radius shows low affinity in relation to both elements,
317 suggesting geochemical control. At this respect, Cánovas et al. (2007) reported on the
318 solubility control of Ba by sulfate in the Odiel waters. The similar trend followed by Pb
319 in relation to Ba also seems to indicate solubility control of this element by sulfate. The
320 sharp decrease in Fe and Cr concentrations concomitant to the discharge peaks (Fig. 3)

may be due to the precipitation of Fe as the pH rises. In this way, sorption processes of Cr onto the Fe precipitates may explain the sharp decrease observed for this element.

Figure 4 shows the mass ratio relationships of some dissolved elements during the study period. These ratios are commonly used in geochemistry to understand the processes influencing the composition of water, such as mixing, precipitation, sorption, etc. If compared with sulfate, which can be considered as conservative in AMD waters (Berger et al. 2000), Fe exhibit a non-conservative behavior as evidenced by the Fe/SO_4 mass ratio. The decrease of Fe concentration in respect to Cu is also evident (Fig. 4). As a consequence of the dilution effect exerted by runoff waters, pH values increased during the survey to greater than 3, leading to Fe hydrolysis reactions. These reactions were especially intense during the discharge peaks when Fe hydroxide complexes ($Fe(OH)_2^+$; Figure 5B) were the dominant Fe species according to geochemical calculations performed with the PHREEQC code (Parkhurst and Appelo, 1999). Saturation indices (SI) revealed values close to equilibrium for jarosite-K, plumbojarosite and schwertmannite during the first discharge rise and slightly undersaturated during the second discharge rise. In turn, waters were undersaturated with respect to jarosite-H, jarosite-Na and ferryhidrite during the entire period (Fig. 5C and D). The lack of an apparent Fe solubility control during the second discharge rise may have been related to the dilution effect of runoff waters which sharply decreased the concentration of Fe, and the predominance of ferrous species (Fig. 5A).

Iron hydrolysis reactions caused the buffering of pH, and even the depletion of Fe from solution, especially during the second discharge rise (Fig. 3). In AMD-affected environments, when Fe is depleted, Al can replace the buffering role of pH. The Al/Zn

346 and Al/Mn mass ratios represented in Figure 4 indicate a sharp decrease in both ratios
347 during the discharge peaks, which could suggest a buffering role by Al. However, the low
348 pH values found in this study (below 4.1) make the precipitation of Al mineral phases
349 improbable. At this respect, geochemical calculations performed with PHREEQC predict
350 the undersaturation of waters with respect to most common Al minerals precipitating in
351 AMD environments (not shown in Fig. 5). Other relationships, shown in Figure 4, such
352 as Cu/Zn seem to indicate a different behavior among these elements, decreasing during
353 the falling limb and increasing during the rising limb. Sorption and coprecipitation
354 processes onto Fe precipitating mineral phases may not be a major cause of these
355 differences, as pH values remain low during these types of reactions (Smith, 1999). These
356 differences could be due instead to a change in the relative contribution from AMD
357 sources and runoff waters. Water enrichment due to Ca in relation to Mg during the
358 discharge rise (Fig. 4) points to the influence of mixing processes on the river
359 hydrochemistry.
360

361 **4.2.2. Mixing processes**

362 The fluctuation in EC values and changes in mass ratios during the survey (Fig. 4) indicate
363 the influence of waters with different mineralization on river water quality. Figure 6
364 shows the influence of the main AMD sources (Table 1) and freshwaters from the study
365 area (Sarmiento, 2008) on the Odiel River hydrochemistry. All elements represented
366 seem to have a quasi-conservative behavior during the study period, as neither
367 precipitation nor sorption processes seem to be observed. The alignment of samples to a
368 hypothetical mixing line between AMD sources and freshwaters (Fig. 6) indicates the
369 influence of mixing processes on the Odiel River. It was noted that Riotinto was the main

source of pollutants (Fig. 6). The high concentrations of Ca in Almagrera lixiviates (Fig. 6) due to neutralization treatments by calcite which decreases the acidity and toxic metal content are also striking.

Despite the high number of pollutant discharges into the Odiel River along the controlled reach, the most important inputs are those from Riotinto Mines (Sarmiento, 2008). Therefore, it is hypothesized that the Odiel river hydrochemistry evolved over the survey through mixing processes of these lixiviates and freshwaters. This hypothesis arises from the natural attenuation processes observed in the Odiel River up to the confluence of the Agrio River (also known as Tintillo), which collects Riotinto lixiviates, causing the irreversible deterioration of the Odiel water quality (Sánchez-España et al., 2006; Sarmiento et al., 2009). In order to confirm this hypothesis, we simulated a two end-member mixing model performed with the MIX code (Carrera et al., 2004) using as end-members, hydrochemical data of Riotinto lixiviates and the Villar Creek before receiving mine lixiviates (Table 3), the latter is an example of a freshwater representative of this catchment. Estimations performed with MIX revealed that between 85% and 98% of the water arriving at the sampling point corresponded to freshwaters (Table 3). These figures highlight the contaminant power of AMD sources, which deteriorate the water quality of the Odiel River with a contribution lower than 15% of its discharge.

From the mixing ratios obtained by MIX, the expected values for each element were calculated, and compared to the measured values in order to identify processes other than mixing that have affected the element concentrations. In general, most elements (Al, Cd, Co, Cu, Li, Mg, Mn, Ni and sulfate; Fig. 7) showed a high correlation (R^2 above 0.95) between the expected and measured values, while lower correlations were observed for

Cr, Ca, Sr and Zn (R^2 between 0.85 and 0.95; the latter not shown in Fig. 7). However, the expected values for Fe were considerably higher than those measured due to the non-conservative behavior exhibited by Fe. Chromium and Pb also had non-conservative behavior. On the one hand, Cr seemed to be affected by sorption processes onto the Fe precipitates, as the expected values were higher than those measured. On the other hand, Pb exhibited the opposite behavior and measured concentrations were higher than expected. This metal has a complex behavior; its solubility seems to be controlled by sulfate concentration (Cánovas et al., 2007). Also preferential coprecipitation with jarosite instead of schwertmannite may occur (Cánovas et al., 2010). Thus, the precipitation of schwertmannite and the low sulfate concentration would enhance Pb solubility. The differences between the expected and measured values for Na were unclear, but may be related to the presence of other sources not controlled in this study.

4.2.3. Influence of the filter size on the determination of the truly dissolved phase

Analytical results revealed higher dissolved concentrations in samples after filtering through 0.45 μm than when using 0.10 μm membranes for Fe, Pb and Cr. These elements, in addition to As, have been reported to be ubiquitous elements in AMD precipitates. As colloid particles aggregate to form more long-term precipitates, it is reasonable to believe that the higher concentrations of Fe, Cr and Pb found in the 0.45 μm phase could be due to these colloid particles. The same procedure was performed in this river under baseflow conditions and there were no differences among elements. Therefore, according to these data it is recommended that 0.10 μm filters should be used to determine Fe concentrations, and to a lesser extent, Cr and Pb in waters affected by AMD during rain events, when an increase in colloid particles is expected. However, according to Kimball et al. (1992), in

Fe-rich systems even 0.10 μm membranes may allow Fe colloids to pass through and be analyzed as part of the dissolved phase, which indicates the importance of ultrafiltration to determine the metal distribution between the dissolved and the particulate phases. In this sense, Sánchez-España et al. (2008) reveals from ultrafiltration studies that around 25% of Fe considered routinely (after 0.45 μm filtration) as dissolved Fe in an acidic pit lake of the IPB was actually present in the solid phase as ferric colloids.

4.2.4. Total concentrations

Dissolved concentrations of most elements decreased with discharge rises during the survey. However, total concentrations (dissolved + particulate) for some elements (Fe, As, Cr, Pb, Ba, Ti and V) followed closely the discharge curve (Fig. 3). Concerning Fe, precipitation during the study period may not be the main source of particulate matter due to the high total concentrations reached (up to 1243 mg/L of Fe; Table 2) with respect to initial dissolved concentrations. Rain events provoke energy inputs which shake and disturb sediments previously deposited on the riverbed. These sediments are composed of large amounts of amorphous or poorly crystalline oxyhydroxides of Fe with minor phyllosilicates (mainly illite/muscovite and kaolinite), quartz, and metallic sulfides (Galán et al., 2003). This sediment load is re-suspended during discharge rises, increasing the particulate matter transported by the river. Sanchez-España et al. (2005) estimated that around 99% of Fe and As, and approximately 60-80% of other metals (Al, Cu, Zn, Cd, Pb, etc) and sulfate released from mine effluents within the Odiel catchment are retained in the sediments. Thus, metals accumulated in Fe and Al mineral phases are remobilized during discharge rises and transported downstream, finally being deposited in estuarine sediments and even in bottom sediments in water reservoirs distributed within the Odiel basin.

445

446 Jarosite and schwertmannite seem to be the most probable precipitating minerals in acidic
447 and oxidizing SO_4-rich waters between pH 2.3 and 3.6 (Bigham et al., 1996), although
448 schwertmannite predominates at pH values between 3 and 4 (Murad and Rojik, 2003). In
449 fact, geochemical modeling predicted SI values close to equilibrium for schwertmannite
450 and jarositic minerals during the first discharge rise (pH between 2.9 and 3.7). The XRD
451 profiles identified the presence of Fe mineral phases in 4 out of 5 samples analyzed, as
452 evidenced by the existence of bands corresponding to schwertmannite (Fig. 8), however,
453 the high abundance of quartz and the low crystallinity of Fe precipitates formed in AMD-
454 affected environments make it difficult to identify such amorphous phases by XRD. At
455 this respect, the presence of Fe hydroxysulfates has been confirmed by SEM (attached as
456 Suplementary Material) as indicates the spherical morphology typical of these mineral
457 phases. Although geochemical calculations by PHREEQC revealed that waters were
458 undersaturated with respect main Al mineral phases, the presence of Al hydroxysulfates
459 was also confirmed by SEM. This suggests that these Al mineral phases precipitated
460 upstream and were carried as suspended load during the rain event. The presence of
461 gypsum in the suspended load during the first discharge peak was also confirmed by XRD
462 (Fig. 8) and SEM images, despite the undersaturation predicted by PHREEQC. This
463 mineral may have been formed in other environments within the catchment, such as AMD
464 pools or stagnant waters that usually exhibit supersaturation, and subsequently carried by
465 the river (as well as Al hydroxysulfates) up to the sampling point as a consequence of the
466 river current energy

467

468 The capacity of Fe and Al hydroxysulfates to remove As, Cr and Pb from solution has
469 been widely reported (e.g. Fukushi et al., 2003; Accornero et al., 2005; Acero et al., 2006;
470 Sánchez-España, 2007), which would explain the high concentrations found in the total
471 fraction. On the other hand, the high concentrations observed for Ti could be caused by
472 the dissolution of phyllosilicates from remobilized sediments during the acid digestion
473 step. This element is the ninth most common in the earth's crust, and is present in
474 abundance in clays with an average content of 0.80 %wt TiO_2 (Dill, 2010). In this way,
475 the XRD profiles revealed the preponderance of silicate particles such as quartz, kaolinite
476 and illite (Fig. 8). This would also explain the presence of Si and Al in the suspended load
477 carried by the river, especially during the discharge peaks when a higher sediment load is
478 transported. During the survey, high total concentrations of Ba were also found (Fig. 3).
479 Although PHREEQC indicated SI values close to equilibrium for barite, this mineral is
480 commonly associated to sulfides in the IPB; therefore its presence in the suspended load
481 is probably linked to weathered material carried by the river. .
482

483 **4.2.5. Pollutant load carried by the river**

484 The dissolved pollutant load was estimated using the following equation:

485 $$L_T = \Sigma \, ½ \, (C_{i\,(n)} + C_{i\,(n+1)}) \, Q_{T\,(n \rightarrow n+1)} \qquad \textit{Eq. 1}$$

486 where L_T is the total load, C_i the pollutant concentration in sample i and Q_T the discharge.

487 Alternatively, a new method is proposed to estimate both the dissolved and total loads,
488 based on high-resolution EC and discharge data recorded by a datalogger. On the one
489 hand, the dissolved load of the elements whose concentrations exhibited a good
490 correlation ($R^2 > 0.89$) with EC values was estimated from EC data recorded by the
491 datalogger, through the establishment of relationships (Fig. 9). The concentration values

obtained were subsequently multiplied by its associated discharge to estimate the total load. A similar method of estimation was used for total concentrations of Fe, As, Cr, Ti, and Ba, according to the high correlations observed between concentration and the river discharge when $R^2 > 0.75$ (Fig. 9). High temporal resolution samplings allow estimating precisely the metal flux in comparison with conventional methods based on low temporal resolution. These methods rely on daily or weekly sampling to calculate the metal load and therefore, do not usually consider the high hydrochemical variability during storm events, leading to overestimation (Olías et al., 2006).

Estimations obtained from Eq. 1 showed a dissolved pollutant load of 226 t of sulfate, 13 of Al, 5.3 of Zn, 3.2 of Mn, around 1.9 of Cu, 1.7 of Fe, and lesser amounts of other metals (92 kg of Co, 47 kg of Ni, etc.; Table 4). Values obtained from established relationships between dissolved concentration and EC were similar to those obtained from Eq. 1, although slightly lower. Table 5 compares dissolved pollutant fluxes recorded in some AMD river systems with those recorded in this study. With the exception of Cd, metal fluxes in the Odiel River were higher than those observed in the Riou Mort (France), the main source of Cd pollution into the Gironde Estuary (Coynel et al. 2007). When compared with pollutant fluxes recorded in Contrary Creek (Colorado, USA), only sulfates, Fe and Cd were higher than those observed in the Odiel River. In both cases (Riou Mort and Contrary Creek), the average discharge was higher than in the Odiel River. However, the highest differences were found when compared with the adjacent Tinto River, with pollutant fluxes between 5 and 20 times higher than in the Odiel, despite carrying similar discharges (Table 5). This was due to the more extreme conditions observed in the Tinto River and to the different hydrogeochemical processes involved during rain events in both rivers. The first rainfalls recorded in the Tinto River after

517 summer caused the dissolution of Fe-rich evaporitic salts and the transport of accumulated
518 pyrite oxidation products from mine sites, while in the Odiel River, rainfalls were
519 recorded during the humid period, causing the dilution of mining pollutants. This can be
520 appreciated by the significant difference in Fe flux between the two rivers, which was
521 almost 200 times higher in the Tinto (Table 5).
522
523 The event monitored in the Odiel River followed a very dry season, with scarce rainfalls,
524 which generated low discharges in relation to other events studied in the area; therefore
525 only covers a reduced period of the hydrological year. In this sense, higher metal fluxes
526 are expected during more humid hydrological years. However, not only hydrological
527 factors must influence metal fluxes in the Odiel River. In this sense, the intense washout
528 processes of soluble salts in October 2005 caused a metal transport by the Tinto River
529 quite similar to that recorded in October 2004, despite having appreciably lower
530 discharges. On the other hand, this study estimates metal loads from dissolved
531 concentration after filtering through 0.45 μm membranes, the most common filter used in
532 AMD waters. According to analytical results, this involves an overestimation of around
533 3-30% for Pb and Cr dissolved load in respect to that estimated after using 0.10 μm filters.
534 The overestimation of Fe load is even higher (30-60%) in most samples, which points the
535 influence of colloids on dissolved metal load estimation in AMD waters during rain
536 events.
537
538 The total pollutant load of those elements, characterized by their presence in the
539 particulate phase, was 61 t of Fe, 1.1 of As, 0.2 of Pb and lesser amounts of Ti and Cr
540 (Table 4). There are few quantitative examples of total or particulate pollutant transport
541 in rivers during rain events, and most report monthly or annual loads, or even

instantaneous loads during floods. This may be due to the difficulty in performing high-temporal resolution sampling and in applying suitable quantifying methodologies. From a high-resolution sampling (3 h), Coynel et al. (2007) reported particulate loads of Cr, As and Pb in the Lot River (France) at around 6000, 600 and 40 times higher, respectively, than in this study, although the discharge carried by the Lot River was almost 2500 times higher.

The application of a quantifying methodology based on EC-C_{diss} and Q-C_{TOT} relationships, allowed a reliable estimate of the metal/loid fluxes in the Odiel River during rainy conditions (Table 4). These figures revealed the transport of total Fe which was 37 times higher than dissolved Fe. Lower values were observed for Pb (7 times higher) and Cr (5 times higher), although the most striking finding was recorded for As, which was totally transported by particulate matter. These figures highlight the importance of the particulate pollutant load during rainy conditions in AMD-affected river systems. Taking into account low discharge values observed during this rain event (maximum of 2.3. m3/s, as the event followed a very dry season), a higher particulate metal load is expected during high-flow conditions, when metal-rich sediments may be significantly carried by the Odiel River.

CONCLUSIONS

This study evaluated the pollutant processes in the Odiel River during rain events. The installation of an EC sensor with a datalogger allowed identification of the arrival of waters with different mineralization at the sampling points, which would otherwise be unnoticed. During the discharge rises, there was a decrease in most dissolved elements due to the dilution effect of runoff waters, Fe being the most affected element due to

567 precipitation processes. The low pH values observed during the study (2.9-4.1) limited
568 sorption and coprecipitation processes onto Fe precipitates; therefore the variations
569 observed among metals may be related to changes in the relative contribution from AMD
570 sources and runoff waters from unaffected points in the basin. The results obtained with
571 the two end-member mixing model proposed in this study approached the measured
572 results. According to this model, the contribution of freshwaters was around 85-98% of
573 the total discharge, highlighting the importance of AMD sources in the deterioration of
574 Odiel water quality, mainly from the Riotinto Mine.
575
576 During the course of the survey, true dissolved concentrations were determined using
577 filters of different pore diameter (0.10 and 0.45 μm). Results revealed similar
578 concentrations of most elements in both fractions. Only Fe, and to a lesser extent, Pb and
579 Cr, showed higher concentrations in the 0.45 μm fraction due to the presence of Fe
580 colloids in the water column.
581
582 Analyses of total concentrations revealed high concentrations of As, Fe, Pb, Cr, Ti V and
583 Ba in the particulate phase due to Fe-rich sediment remobilization, and to a lesser extent,
584 direct precipitation. These amorphous Fe precipitates are efficient sinks of other
585 pollutants such as As, Pb, Cr, V, etc., which are transported downstream during flood
586 events. Other elements such as Al, Cu, Li, Ni, Si, Sr and sulfate were only present in the
587 particulate phase during the discharge peaks. No differences were found between the
588 dissolved and total concentrations for the remaining elements.
589
590 Both the dissolved and the total pollutant loads were estimated by different methods.
591 During the study period (8 days), a dissolved pollutant load of 226 t of sulfate, 13 t of Al,

5.3 t of Zn, 3.2 t of Mn, around 1.9 t of Cu, 1.7 t of Fe, and lesser amounts of other metals (92 kg of Co, 47 kg of Ni, 24 kg Pb, 17 kg of Cd, etc.) was transported by the Odiel River. However, the presence of colloids (between 0.1 and 0.45 μm) involve an overestimation of around 3-30% of Pb and Cr load, and of 30-60% of Fe load carried by the Odiel River during this study, suggesting the need of using filters with smaller size to perform routinely metal estimations in AMD waters during rain events.

On the other hand, almost 61 t of Fe, 1.1 t of As, 0.2 t of Pb and lesser amounts of Cr and Ti were transported in the total (dissolved and particulate) fraction, which implies the transport of total Fe which is 37 times higher than dissolved Fe, almost 7 times higher for Pb and 5 times higher for Cr. In the case of As, this element was totally transported by particulate matter. Therefore, rain events decrease dissolved pollutant concentrations, however, this can result in an increase in the particulate concentration of some toxic elements (As, Pb, Cr, etc.) and in dissolved pollutant load.

ACKNOWLEDGEMENTS

This work has been financed by the Spanish Ministry of Education and Science through project CGL2010-21956-C02. CRC was financially supported by the Spanish Government with a research contract within the "Juan de la Cierva" program. The authors wish to thank the Environmental Council of the Andalusian Regional Government for the information provided for this study. We are grateful to John Selker, three anonymous reviewers and the associate editor Heidi Nepf for their insightful comments.

REFERENCES

Accornero M., L. Marini, G. Ottonello and M. Vetuschi Zuccolini (2005). The fate of major constituents and chromium and other trace elements when acid waters froom the derelict Libiola mine (Italy) are mixed with stream waters. *Appl. Geochem*., 20, 1368-1390; doi:10.1016/j.apgeochem.2005.03.001

Acero P., Ayora, Torrentó C and Nieto J.M (2006). The behavior of trace elements during schwertmannite precipitation and subsequent transformation into goethite and jarosite. *Geochim. Cosmochim. Ac.*, 70, 4130-4139, doi:10.1016/j.gca.2006.06.1367

640 Allison JD, Brown DS, Novo-Gradac KJ. (2003) MINTEQA2/PRODEFA2. A
641 geochemical assessment model for environmental systems. Version 3.0.
642 Environmental Research Laboratory, Office of Research and Development, U.S.
643 Environmental Protection Agency. Athens (Georgia)

644 Audry, S, Blanc, G and Schäfer, J (2005). The impact of sulphide oxidation on dissolved
645 metal (Cd, Zn, Cu, Cr, Co, Ni, U) inputs into the Lot–Garonne fluvial system
646 (France). *Appl. Geochem.*, 20, 919-931. doi:10.1016/j.apgeochem.2005.01.006

647 Berger, AC, Bethke, CM, Krumhansl, ML, (2000). A process model of natural
648 attenuation in drainage from a historic mining district. *Appl. Geochem.*, 15, 655-
649 666.

650 Bigham J.M., U. Schwertmann, S.J. Traina, R.L. Winland and M. Wolf (1996).
651 Schwertmannite and the chemical modeling of iron in acid sulfate waters. *Geochim.*
652 *Cosmochim. Ac.,* 60(12), 2111-2121.

653 Bigham, J.M. and D.K. Nordstrom (2000). Iron and Aluminium-Hydroxysulfate
654 Minerals, in *Sulfate Minerals. Crystallography, Geochemistry and Environmental*
655 *Significance. Reviews in Mineralogy and Geochemistry*, v.40, Mineralogical
656 Society of America, edited by C.N. Alpers, J.L. Jambor, and D.K. Nordstrom,
657 Washington D.C.

658 Blowes D.W., C.J. Ptacek, J.L. Jambor and C.G. Weisener (2004). The geochemistry of
659 acid mine drainage, in *Treatise on geochemistry. Environmental geochemistry*, v9,
660 Elsevier, edited by B.S. Lollar, 149-204.

661 Braungardt C.B., E.P. Achterberg, F. Elbaz-Poulichet and N.H. Morley (2003). Metal
662 geochemistry in a mine polluted estuarine system in Spain. *Appl. Geochem.*, 18,
663 1757-1771, doi:10.1016/S0883-2927(03)00079-9.

664 Cánovas C.R., M. Olias, J.M. Nieto, A.M. Sarmiento and J.C. Cerón (2007).
665 Hydrogeochemical characteristics of the Odiel and Tinto rivers (SW Spain). Factors
666 controlling metal contents. *Sci. Total Environ.* 373, 363-382,
667 doi:10.1016/j.scitotenv.2006.11.022

668 Cánovas C.R, C.G. Hubbard, M. Olías, J.M. Nieto, S. Black. and M.L. Coleman (2008).
669 Hydrochemical variations and contaminant load in the Río Tinto (Spain) during
670 flood events. *J. Hydrol.*, 350 (1-2), 24-40, doi:10.1016/j.jhydrol.2007.11.022

671 Cánovas, C.R., M. Olías, J.J. Nieto, and L. Galván (2010). Wash-out processes of
672 evaporitic sulfate salts in the Tinto River: hydrogeochemical evolution and
673 environmental impact. *Appl. Geochem.*, 25, 288-301,
674 doi:10.1016/j.apgeochem.2009.11.014

675 Carrera, J., E. Vázquez-Suñé, O. Castillo and X. Sánchez-Vila, (2004). A methodology
676 to compute mixing ratios with uncertain end-members. *Water Resour. Res.*, 40,
677 W12101, doi:10.1029/2003WR002263.

678 Coynel, A., Schäfer, J., Blanc, G. and Bossy, C. (2007). Scenario of particulate trace
679 metal and metalloid transport during a major flood event inferred from transient
680 geochemical signals. *Appl. Geochem.,* 22, 821-836.

681 Davis J.C. (1986). *Statistics and data analysis in Geology*. John Wiley and sons. New
682 York.

683 Dill, H.G. (2010). The "chessboard" classification scheme of mineral deposits:
684 Mineralogy and geology from aluminum to zirconium. *Earth-Sci. Rev,* 100, 1-420,
685 doi:10.1016/j.earscirev.2009.10.011

686 Fukushi K., M. Sasaki, T. Sato, N. Yanase, H. Amano, and H. Ikeda (2003). A natural
687 attenuation of arsenic in drainage from an abandoned mine dump. *Appl. Geochem,*
688 18, 1267–78, doi:10.1016/S0883-2927(03)00011-8.

689 Galán E., J.L. Gómez-Ariza, I. González, J.C. Fernández-Caliani, E. Morales and I.
690 Giráldez (2003). Heavy metal partitioning in river sediments severely polluted by
691 acid mine drainage in the Iberian Pyrite Belt. *Appl. Geochem.*18, 409-421.

692 Garbarino J.R. and G.L. Hoffman (1999). Methods of Analysis by the U.S. Geological
693 Survey National Water Quality Laboratory. Comparison of a nitric acid in-bottle
694 digestion procedure to other whole-water digestion procedures. *Open File Report*
695 *99-094*, US Geological Survey. Denver, Colorado.

696 García de Miguel, J.M., (1990). Mineralogía, paragénesis y sucesión de los sulfuros
697 masivos de la Faja Pirítica en el suroeste de la Península Ibérica. *Bol. Geol. Min.,*
698 101, 73–105.

699 Hoffman, G.L., M.J. Fishman and J.R. Garbarino (1996). Methods of analysis by the
700 U.S. Geological Survey National Water Quality Laboratory. In-bottle acid-
701 digestion of whole-water samples. *Open-File Report 96-225.* U.S. Geological
702 Survey. Denver, Colorado.

703 Kimball B.A., D.M. McKnight, G.A. Wetherbee and R.A. Harnish (1992). Mechanisms
704 of iron photoreduction in a metal-rich acidic stream (St. Kevin Gulch, Colorado.
705 U.S.A.). *Chem. Geol.,* 96,227-239.

706 Langmuir D. (1997). *Aqueous environmental geochemistry*. Prentice Hall, Upper Saddle
707 River.

708 Murad E. and P. Rojik (2003). Iron-rich precipitates in a mine drainage environment:
709 influence of pH on mineralogy. *Am. Mineral.*, 88, 1915–1918.

710 Nieto J.M., A.M. Sarmiento, M. Olías, C.R. Cánovas, I. Riba, J. Kalman and T.A.
711 Delvalls (2007). Acid mine drainage pollution in the Tinto and Odiel rivers (Iberian
712 Pyrite Belt, SW Spain) and bioavailability of the transported metals to the Huelva
713 estuary. *Environ. Int.* 33, 445-455, doi:10.1016/j.envint.2006.11.010.

714 Nocete F., E. Alex, J.M. Nieto, R. Sáez and M.R. Bayona (2005). An archaelogical
715 approach to regional environmental pollution in the south-western Iberian
716 Peninsula related to Third Millenium B.C mining and metallurgy. *J. Archaeol.*
717 *Science*, 32 (10), 1566-1576. doi:10.1016/j.jas.2005.04.012

718 Nordstrom D.K and F.D. Wilde (1998). Reduction–oxidation potential (electrode
719 method), in *National field manual for the collection of water quality data, U.S.*
720 *Geological Survey techniques of water-resources investigations*, book 9; chapter
721 6.5.

722 Olías M., J.M. Nieto, A.M. Sarmiento, J.C. Cerón and C.R. Cánovas (2004). Seasonal
723 water quality variations in a river affected by acid mine drainage: The Odiel river
724 (south west Spain). *Sci. Total Environ.*, 333, 267-281,
725 doi:10.1016/j.scitotenv.2004.05.012.

726 Olías M., C.R. Cánovas, J.M. Nieto and A.M. Sarmiento (2006). Evaluation of the
727 dissolved contaminant load transported by the Tinto and Odiel rivers (South West
728 Spain). *Appl. Geochem.*, 21, 1733-1749, doi:10.1016/j.apgeochem.2006.05.009.

729 Parkhurst D.L. and C.A.J. Appelo (1999). User's guide to PHREEQC (Version 2). A
730 computer program for speciation, batch reaction, one-dimensional transport, and
731 inverse geochemical calculations. *USGS water-resources investigations report 99-*
732 *4259*. Denver, Colorado.

733 Pinedo, I. (1963). Piritas de Huelva. Su historia, minería y aprovechamiento. Ed.
734 Summa. Madrid, Spain. 1003 pp.

735 Ruiz M.J., R. Carrasco, R. Pérez-López, A.M. Sarmiento and J.M. Nieto (2003).
736 Optimización del análisis de elementos mayores y traza mediante UN-ICP-OES en
737 muestras de drenaje ácido de mina. *Proceedings IV Iberian Geochemical Meeting*,
738 402–404. July 14th-18th, Coimbra, Portugal. Universidade de Coimbra.

739 Sainz A., J.A. Grande and M.L de la Torre (2004). Characterisation of heavy metal
740 discharge into the Ria of Huelva. *Environ Int.*, 30, 557-566.
741 doi:10.1016/j.envint.2003.10.013.

742 Sanchez España J., E. Lopez Pamo, E. Santofimia, O. Aduvire, J. Reyes and D. Barettino
743 (2005). Acid mine drainage in the Iberian Pyrite Belt (Odiel river watershed,
744 Huelva, SW Spain): Geochemistry, mineralogy and environmental implications.
745 *Appl Geochem*, 20, 1320-1356, doi:10.1016/j.apgeochem.2005.01.011.

746 Sánchez-España J., E. López-Pamo, E. Santofimia, J. Reyes and J.A. Martín-Rubí
747 (2006). The impact of acid mine drainage on the water quality of the Odiel River
748 (Huelva, Spain): Evolution of precipitate mineralogy and aqueous geochemistry
749 along the Concepción-Tintillo segment. *Water Air Soil Poll*, 173, 121-149,
750 doi:10.1007/s11270-005-9033-6.

751 Sánchez-España J., E. López-Pamo, E. Santofimia and M. Diez-Ercilla (2008). The
752 acidic mine pit lakes of the Iberian Pyrite Belt: An approach to their physical
753 limnology and hydrogeochemistry. *Appl Geochem,* 23, 1260–1287,
754 doi:10.1016/j.apgeochem.2007.12.036

755 Sánchez-España, J. (2007). The behavior of iron and aluminum in acid mine drainage:
756 speciation, mineralogy, and environmental significance, in *Thermodynamics,*
757 *Solubility and Environmental Issues*, Elsevier, edited by T.M Letcher, 137-150.

758 Sarmiento, A.M. (2008). Study of the pollution by acid mine drainage of the surface
759 waters in the Odiel basin (SW Spain). M.S. thesis, Department of Geology,
760 University of Huelva, Spain. UMI ProQuest, Publ. No.: AAT 3282346. Ann Arbor,
761 USA.
762 http://proquest.umi.com/pqdweb?did=1404342661&sid=3&Fmt=2&clientId=404
763 00&RQT=309&VName=PQD.

764 Sarmiento A.M., Olías M., Nieto J.M., Cánovas C.R. (2009). Hydrochemical
765 characteristics and seasonal influence on the pollution by acid mine drainage in the
766 Odiel river Basin (SW Spain). *Appl. Geochem.* 24, 697-714,
767 doi:10.1016/j.apgeochem.2008.12.025

768 Smith, K.S. (1999). Metal sorption on mineral surfaces: an overview with examples
769 relating to mineral deposits, in *The Environmental Geochemistry of Mineral*
770 *Deposits*, Rev. Econ. Geol. 6A, edited by G.S. Plumlee and M.J. Logson. pp. 161–
771 182.

772 Yu J.Y., B. Heo, I.K. Choi, J.P. Cho and H.W. Chang (1999). Apparent solubilities of
773 schwertmannite and ferrihydrite in natural stream waters polluted by mine drainage.
774 *Geochim. Cosmochim. Ac.*, 63(19/20), 3407-3416.

775

776

777

778

779

780

781

782

783 **FIGURE CAPTIONS**

784

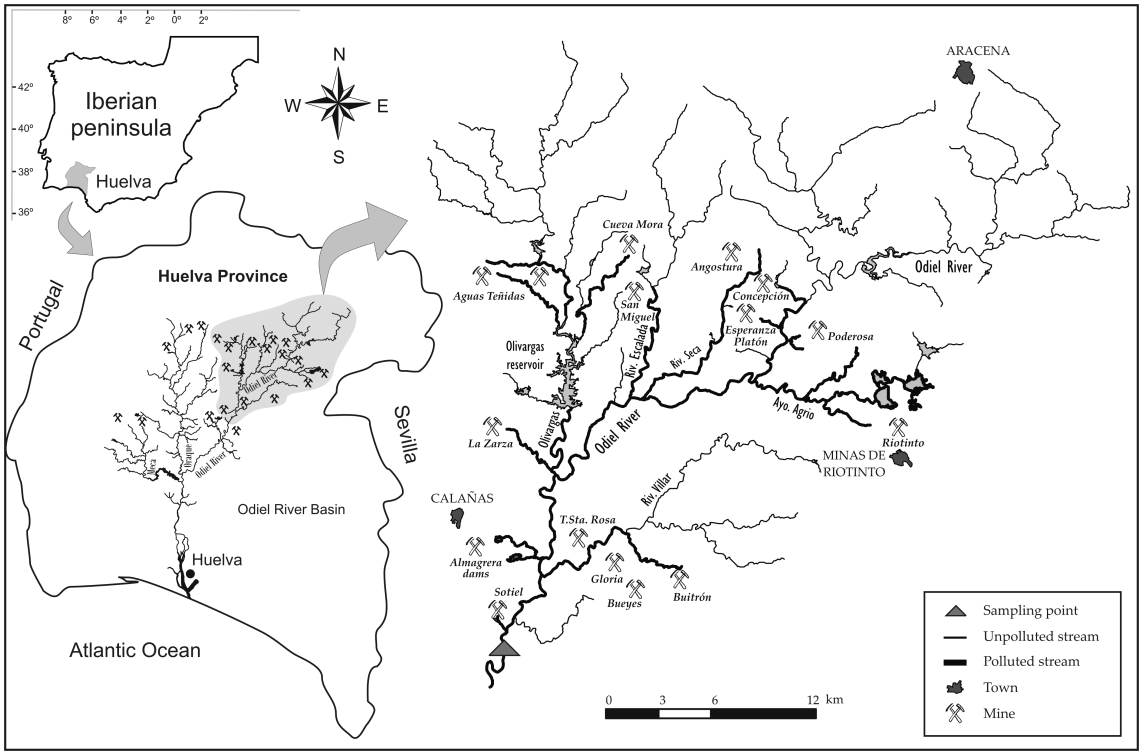

785

786 **Figure 1.** Odiel River location map, indicating the sampling point, the main mines and

787 the AMD affected water courses.

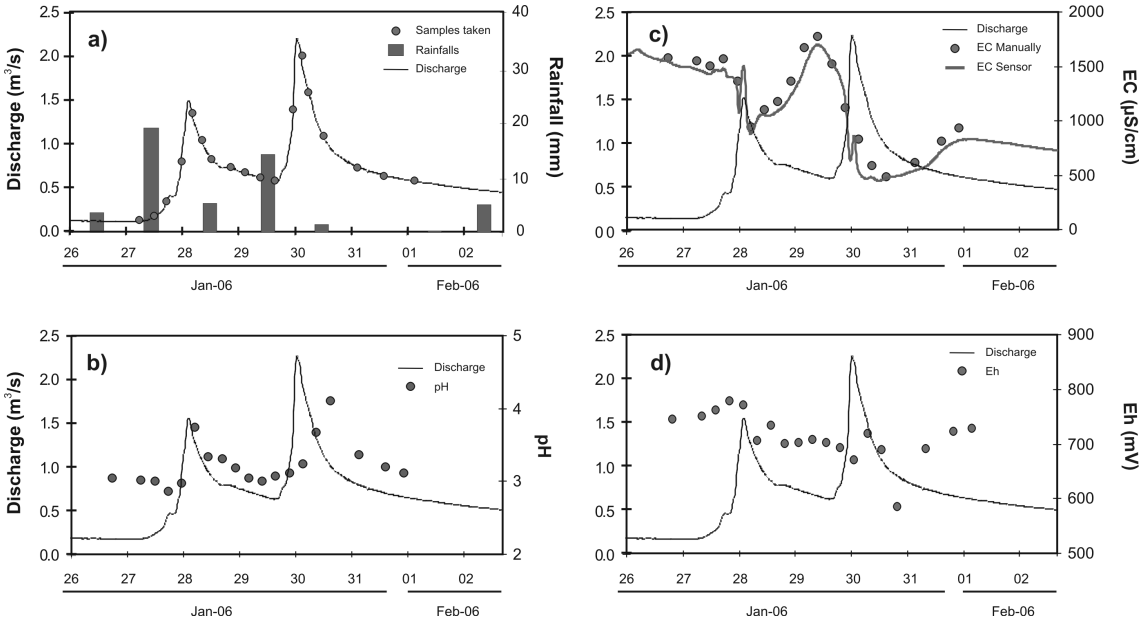

788

789 **Figure 2.** Hydrograph indicating a) rainfall distribution before the event, b) Electrical

790 Conductivity before the event c) rainfall distribution and samples taken during the survey,

791 d) pH, e) Electrical Conductivity (EC) and f) potential redox (Eh) evolution.

792

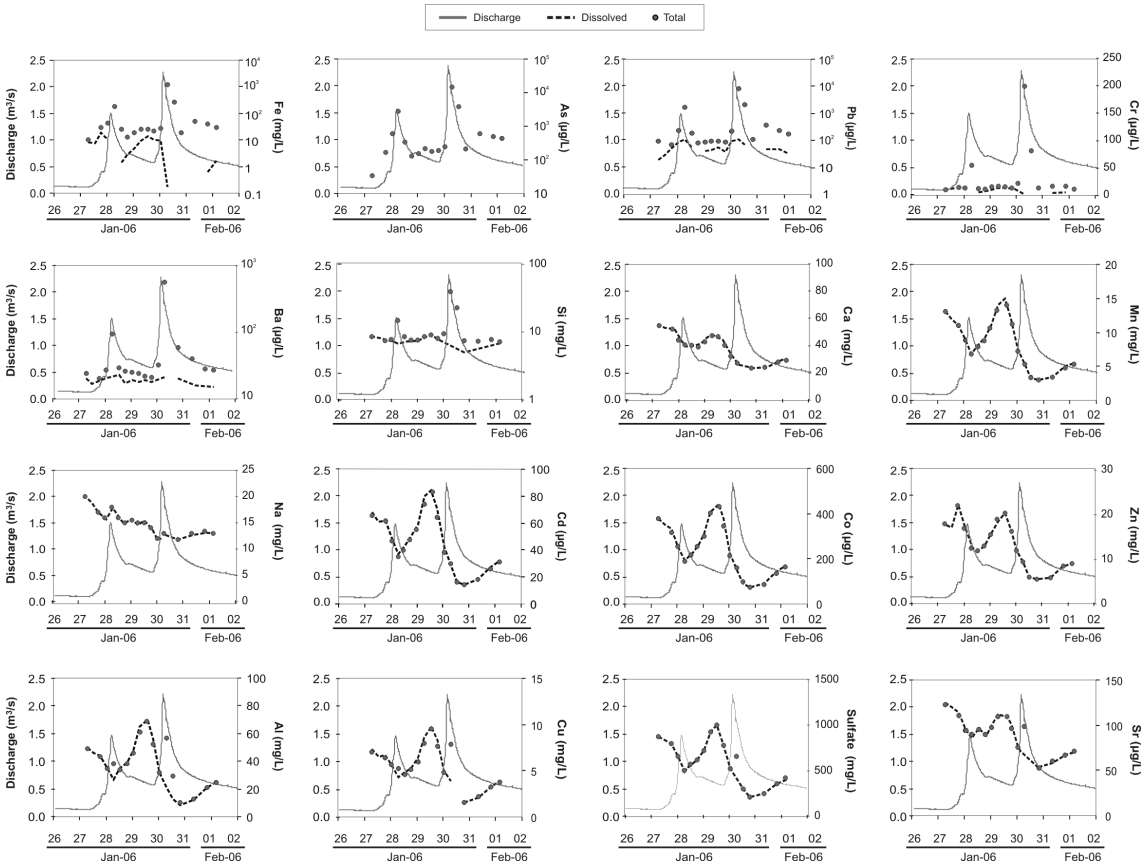

793

794 **Figure 3.** Evolution of the dissolved and total (dissolved + total) concentration of some

795 elements studied during the survey (see text for explanation).

796

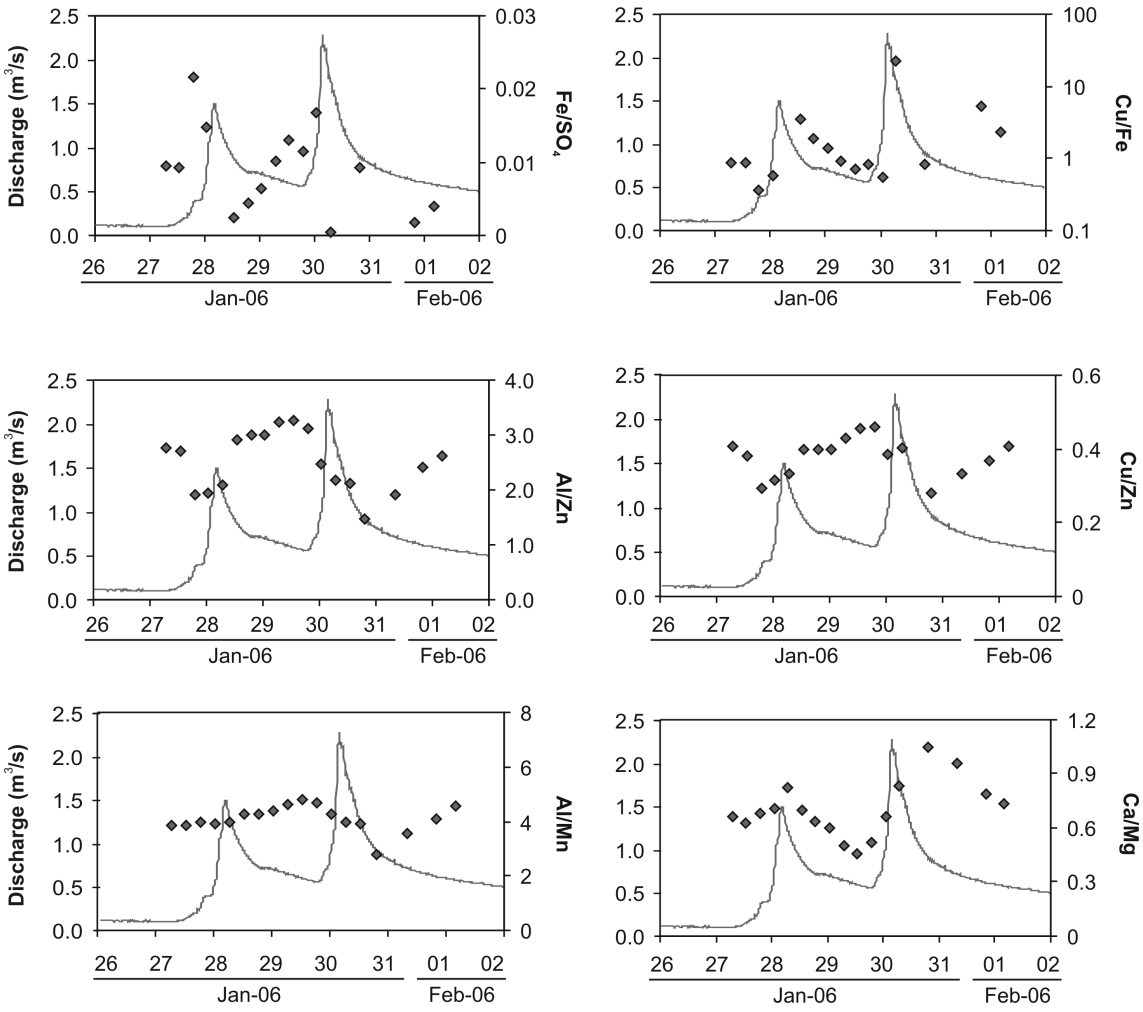

797

798 **Figure 4.** Evolution of mass ratios of some dissolved elements during the survey.

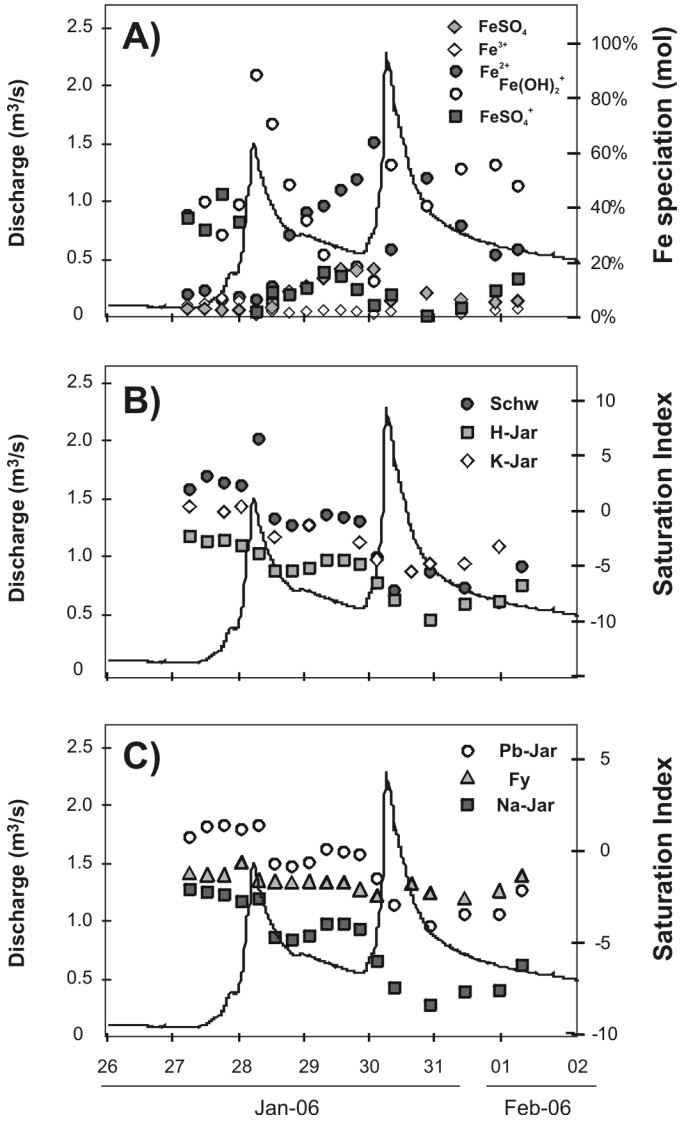

799

800 **Figure 5.** Iron speciation (a and b) and saturation indices of some of the typical Fe
801 precipitating minerals in AMD environments (c and d) in the survey. Ks used for
802 schwertmannite was obtained from Yu et al. (1999).

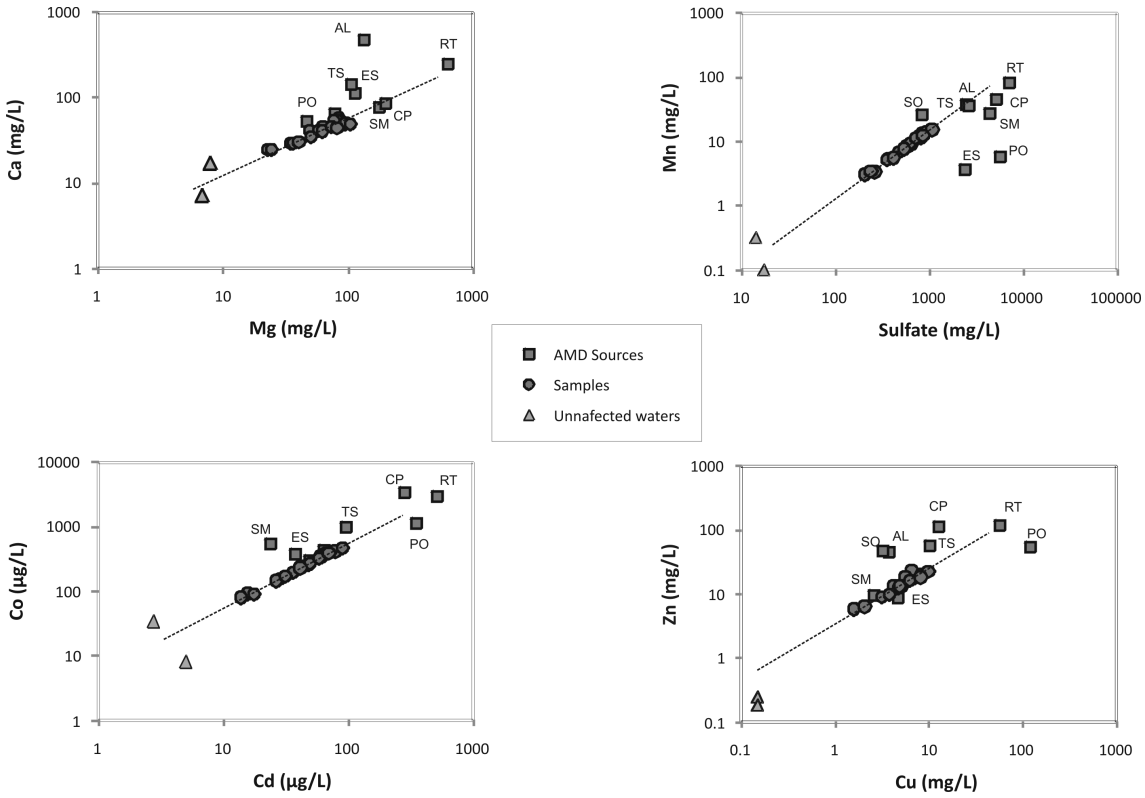

803

804 **Figure 6.** Influence of sources on the Odiel River hydrochemistry over the survey (RT:

805 Riotinto; AL: Almagrera Dams; CP: Concepción; SO: Sotiel; SM: San Miguel; ES:

806 Esperanza; PO: Poderosa; TS: Tinto Sta. Rosa)

807

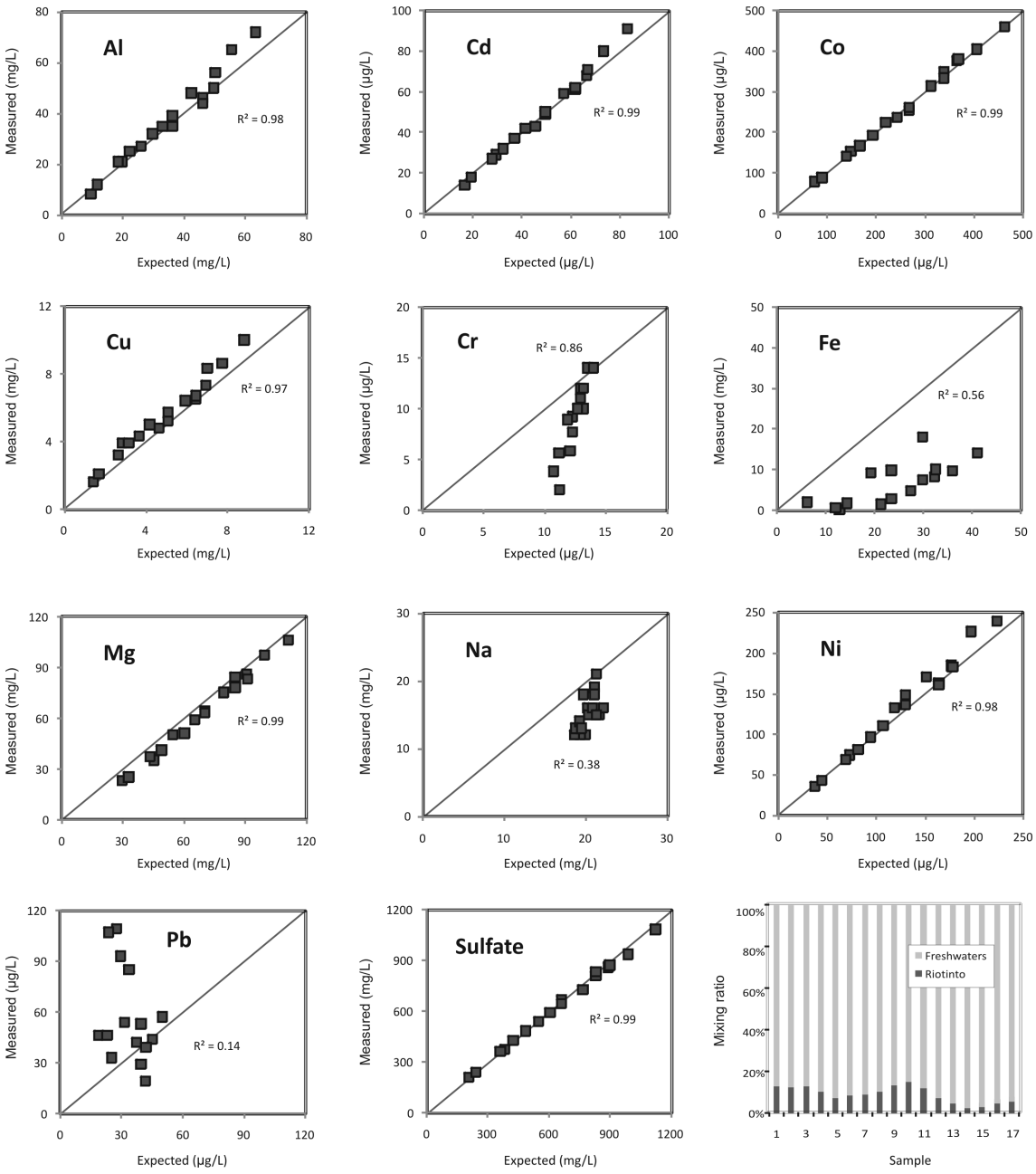

808

809 **Figure 7.** Comparison between measured and expected values from mixing ratios
810 obtained by MIX code (Carrera et al. 2004) from the 2 end-member mixing proposed
811 model.

812

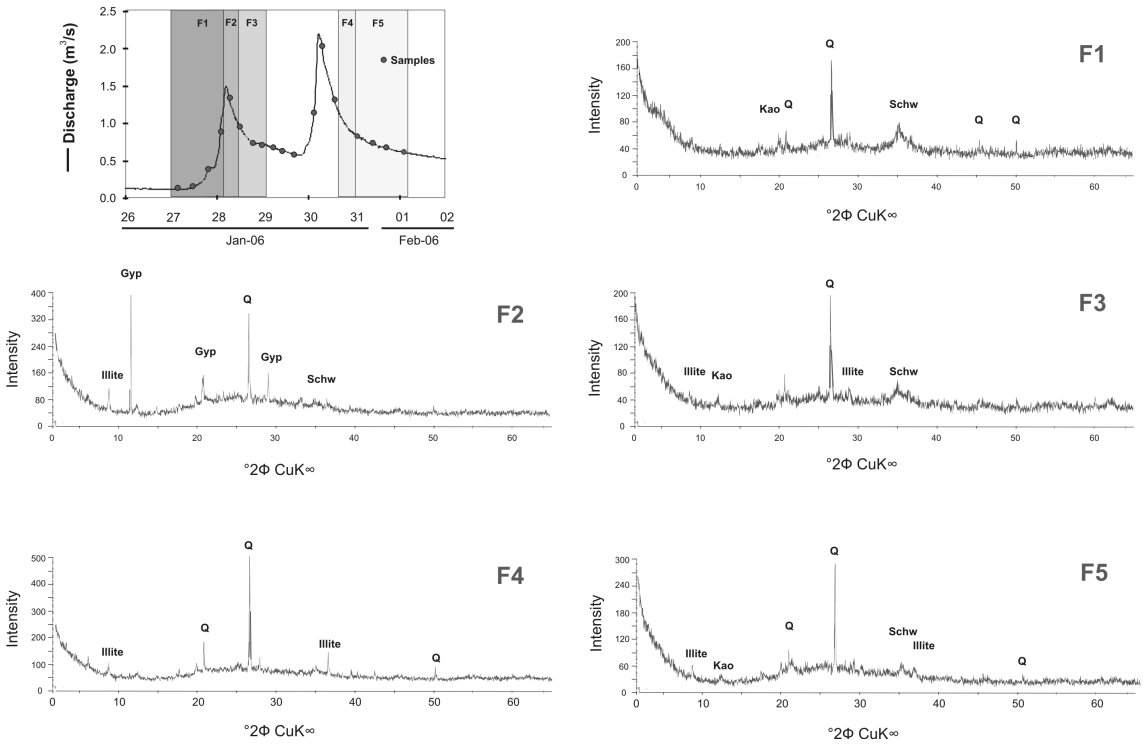

813

814 **Figure 8.** XRD patterns of particulate matter retained during sample filtration.

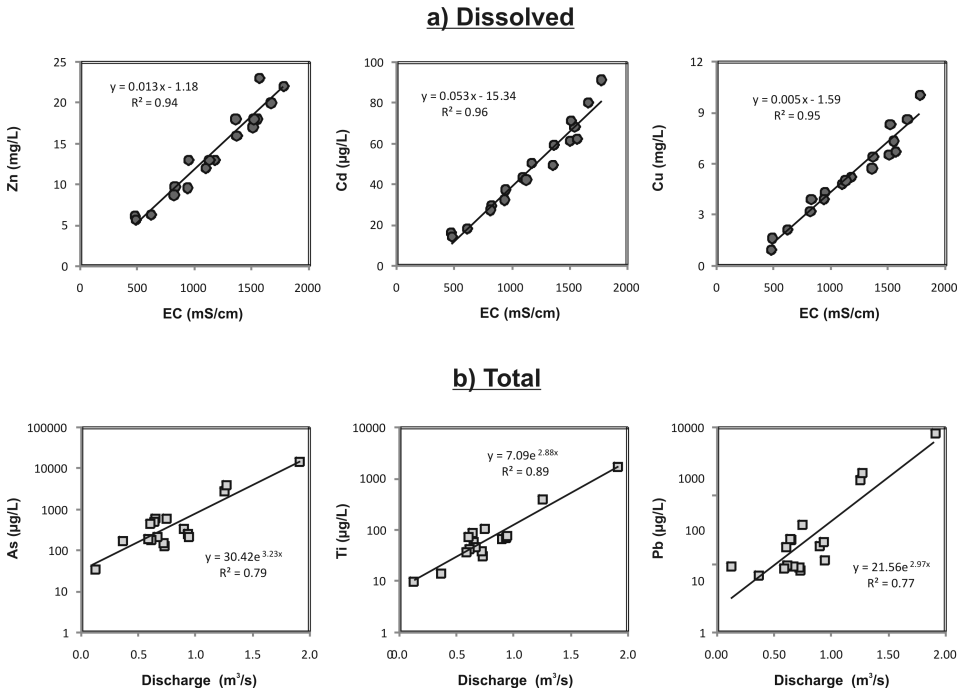

815

816 **Figure 9.** Examples of relationships between a) dissolved concentrations and EC

817 (circles), and b) total concentrations and discharge (squares).

818

819 # TABLE CAPTIONS

Mines (explotation years)[1]	**Minerals**[(1)]	**Ore production**[(1)] (million t)	**Lixiviate composition (mg/L)**[2] Al	Cu	Fe	Zn	SO_4	**Contaminant load (t/year)**[(2)] Al	Cu	Fe	Zn	SO_4
Concepción (1853-1690)	Py, Ch, Ar, Ga	>1	157		1089	112	5100					
Esperanza (1906-1931)	Py, Ch,	1,8			629		2400					
La Poderosa (1864-1924)	Py, Ch, Ca, Co	0,6	4,7		1300		5700					
Riotinto (imprecise)	Pyrite Chalcopyrite	500-600	411		266	121			824		1200	76000
San Miguel (1859-1960)	Pyrite Chalcopyrite Sphalerite Galena	1,3	262		1205		4420			203	5,4	1900
La Zarza	Pyrite Galena Sphalerite Arsenopyrite	27			233		2250			228	11	1500
Almagrera dams	Sulfide wastes				95		2600	253	55	957	401	30200
Tinto S Rosa (1901-1931)	Pyrite Chalcopyrite Arsenopyrite	1,42 (1901-1931)			594		2400					
Sotiel (imprecise)	Polymetallic sulfides	75,2			39		920					

[(1)]Pinedo, 1963;
820 [(2)]Sarmiento et al., 2008

821 **Table 1.** Description of the main mines affecting the drainage basin of the sampling point.

		D.L	n	Mean	Median	Est. Dev.	C.V	Min.	Max.	Perc. 25	Perc. 75
Flow	(m^3/s)		1152	0,63	0,59	0,40	65%	0,12	2,3	0,45	0,75
EC_1	µS/cm	10	18	1186	1176	399	34%	489	1778	885	1538
EC_2	µS/cm	10	1152	1051	925	405	39%	448	1698	744	1470
pH		0,01	18	3,2	3,1	0,31	10%	2,9	4,1	3,0	3,3
Eh	mV	1,0	18	505	499	44	9%	378	574	491	532
						Dissolved					
Al	Main Elements (mg/L)	0,10	18	36	35	18	50%	8,3	72	22	48
Ca		0,12	18	38	41	10	26%	24	57	29	47
Cu		0,11	17	5,5	5,2	2,3	42%	1,6	10	3,9	6,7
Fe		0,10	15	6,6	7,5	5,3	80%	0,17	18	1,8	10
K		0,30	6	1,7	1,7	0,40	24%	1,3	2,2	1,3	2,0
Mg		0,10	18	60	61	26	43%	23	106	38	82
Mn		0,10	18	8,6	8,6	3,8	45%	3,0	15	5,4	12
Na		0,05	17	15	15	2,6	17%	12	21	13	16
Sulfate		0,50	18	606	618	261	43%	207	1083	386	827
Si		0,20	18	7,4	7,4	1,2	16%	5,1	9,5	6,8	8,3
Zn		0,10	18	14	13	5,5	39%	5,7	23	10	18
Ba	Trace Elements (µg/L)	2,0	17	19	19	2,2	12%	15	23	17	20
Cd		1,1	18	47	46	22	48%	14	91	30	62
Co		1,1	18	251	246	118	47%	79	460	157	346
Cr		1,0	14	9,0	10	3,7	41%	2,0	14	6,3	12
Li		1,2	15	75	76	32	42%	18	128	52	94
Ni		1,4	18	128	134	62	48%	35	239	76	168
Pb		2,0	16	58	50	27	47%	19	109	41	72
Sn		3,4	3	6,5	7,2	1,5	23%	4,8	7,5	6,0	7,4
Sr		1,0	17	91	96	23	25%	54	125	70	112
Ti		1,0	18	5,4	4,8	1,7	31%	3,4	9,6	4,4	6,1
V		1,0	8	51	51	10	20%	36	67	44	57
						Total					
Al	Main Elements (mg/L)	0,10	17	41	40	17	43%	11	73	31	52
Ca		0,12	16	40	42	10	25%	23	56	30	47
Cu		0,11	16	5,9	5,8	2,3	40%	1,7	10	4,7	7,6
Fe		0,10	17	125	29	297	238%	10	1243	22	47
K		0,30	6	3,2	1,7	3,3	104%	1,7	10	1,7	2,2
Mg		0,10	17	60	58	25	42%	23	105	42	77
Mn		0,10	17	8,5	8,4	3,8	45%	3,1	15	5,6	12
Na		0,05	16	16	15	2,5	16%	12	21	14	17
Sulfate		0,50	17	633	655	254,2	40%	210	1065	448	827
Si		0,20	17	12	8,7	8,9	74%	7,7	42	8,2	10
Zn		0,10	17	14	13	5,6	41%	5,6	23	10	18
As	Trace Elements (µg/L)	3,2	16	1681	315	3865	230%	139	15537	195	635
Ba		2,0	16	71	29	143	202%	21	601	25	36
Cd		1,1	17	46	41	22	48%	15	88	32	66
Co		1,1	17	251	229	119	47%	81	459	169	334
Cr		1,0	15	36	16	53	147%	11	211	14	21
Li		1,2	16	71	73	34	47%	10	139	53	85
Ni		1,4	17	132	134	60	45%	42	246	82	172
Pb		2,0	17	881	186	2100	238%	71	8653	100	246
Sn		3,4	5	48	10	88	184%	3,1	205	6,1	15
Sr		1,0	16	95	100	21	22%	56	130	79	107
Ti		1,0	17	177	61	423	239%	4,0	1774	39	82
V		1,0	10	187	77	291	155%	44,5	1003	70	135

822

823

824 **Table 2**. Basic statistic of results obtained from dissolved and total concentration
825 analysis. Flow data obtained from sensor readings. EC_1: Electrical Conductivity values
826 obtained manually; EC_2: Electrical Conductivity values obtained from sensor readings

827

Element	End-Members		Sample	Mixing ratios	
	Riotinto	Freshwaters		Riotinto	Freshwaters
Al (mg/L)	411	0,10	S1	0,12	0,88
Ca (mg/L)	249	25	S2	0,11	0,89
Cu (mg/L)	57	0,10	S3	0,11	0,89
Fe (mg/L)	266	0,10	S4	0,09	0,91
Mg (mg/L)	637	16	S5	0,06	0,94
Mn (mg/L)	83	0,10	S6	0,08	0,92
Na (mg/L)	45	18	S7	0,09	0,91
SO_4 (mg/L)	7024	48	S8	0,10	0,90
Zn (mg/L)	121	0,01	S9	0,14	0,87
			S10	0,15	0,85
Cd (µg/L)	512	5,0	S11	0,12	0,88
Co (µg/L)	2967	8,0	S12	0,07	0,93
Cr (µg/L)	36	10	S13	0,05	0,95
Li (µg/L)	872	15	S14	0,02	0,98
Ni (µg/L)	1428	5,0	S15	0,03	0,97
Pb (µg/L)	259	12	S16	0,05	0,96
Sr (µg/L)	2005	60	S17	0,05	0,95

828

829 **Table 3.** End-members composition and mixing ratios obtained by MIX.

830

		Dissolved		Total
		a	*b*	c
Al	*Major elements (ton)*	13	11	-
Cu		1,9	1,3	-
Fe		1,7	-	61
Mn		3,2	2,6	-
Sulfate		226	193	-
Zn		5,3	4,6	-
As	*Trace elements (kg)*	-	-	1134
Cd		17	14	-
Co		92	77	-
Cr		2,2	1,9	11
Ni		47	39	-
Pb		24	-	161
Ti		2,2	-	141

a calculated from Eq. 1

b calculated from EC-concentration relationships

c calculated from Q-concentration relationships

831

832 **Table 4.** Pollutant load transported by the Odiel River during the survey.

833

		Contrary Creek	Riou Mort	Tinto River	Tinto River	Odiel River
		Kimball et al. 2002	Audry et al. 2005	Cánovas et al. 2008	Cánovas et al. 2010	This study
Discharge	m^3/s	0,70	2,1	12	0,83	0,56
Al	$ton\ d^{-1}$	0,54	0,01	14	13	1,6
Cu		0,01		3,2	2,9	0,24
Fe		1,1		25	42	0,21
Mn		0,23		2,3	1,6	0,40
Sulphate		36	24	184	268	28
Zn		0,11	0,26	3,2	3,3	0,66
Cd	$kg\ d^{-1}$	5,5	3,4	16	17	2,1
Co		-	0,50	106	96	12
Cr		-	0,08	3,2	5,6	0,28
Ni		5,8	1,8	32,0	40	5,9
Pb		-		219	36	3,0

Pollutant fluxes and discharge data are expressed as average values

834

835 **Table 5.** Comparison of pollutant fluxes estimated in the Odiel River with other AMD-

836 affected systems.